TTGs in the making: Natural evidence from Inyoni shear zone (Barberton, South Africa)

A. Nédélec, Magdalena Oryaëlle Chevrel, Jean-François Moyen, J. Ganne, S. Fabre

TTGs in the making: Natural evidence from Inyoni shear zone (Barberton, South Africa)

A. Nédélec [a,*], M.O. Chevrel [a,b], J.F. Moyen [c,d], J. Ganne [a], S. Fabre [e]

[a] GET-UMR5563, OMP, Université de Toulouse, 14 avenue Edouard-Belin, 31400 Toulouse, France
[b] Department of Earth and Environmental Sciences, Ludwig Maximilians Universität, Theresienstr.41/III, 80333 Munich, Germany
[c] LMV-UMR6524, Université de Saint-Etienne, 23 rue du Dr Michelon, 42023 Saint-Etienne, France
[d] Department of Earth Sciences, University of Stellenbosch, Western Cape, South Africa
[e] IRAP-UMR5277, OMP, Université de Toulouse, 14 avenue Edouard-Belin, 31400 Toulouse, France

Keywords:
Amphibolite
Archaean
Melting
Garnet
TTG
Cumulate

A B S T R A C T

Despite the consensus that TTGs, the main constituents of the Archaean continental crust worldwide, originated by partial melting of garnet-bearing amphibolites, natural evidence is scarce. A large variety of Archaean amphibole-rich rocks, including migmatitic amphibolites and hornblende-rich cumulates, was exhumed as a tectonic melange in the Inyoni shear zone (ISZ) near Barberton (South Africa), likely at the time of emplacement of the 3.2 Ga Nelshoogte–Badplaas plutons. This unique collection provides the opportunity to investigate partial melting of garnet-amphibolites, as well as the differentiation processes occurring in the TTG magmas en route to the surface. The ISZ migmatitic amphibolites are characterized by quartz-plagioclase leucosomes in equilibrium with garnet, amphibole, titanite ± epidote. Garnet compositions are characterized by high almandine and grossular contents. Actually, the leucosomes and neosomes likely lost part of their melt component and mesosomes may have been also modified towards restite-rich compositions due to melt segregation. Restite-bearing rocks are very iron-rich according to their high contents in garnet. Besides, the Mg-rich compositions of the hornblende cumulates and their REE distribution patterns resemble those of the nearby TT (tonalite–trondhjemite) plutons.
Thermobarometric estimates from the ISZ migmatitic rocks cluster in the range 720–800 °C and 1.1–1.2 GPa for the melting reaction and the derived geothermal gradient is ca 17–22 °C/km. These conditions are consistent with either water-present melting or, more likely, water-absent epidote-dehydration melting. Such a geothermal gradient is therefore assigned to the genesis of large volumes of medium-pressure TTG magmas, that will likely form at greater depth. Unmelted garnet-bearing amphibolites correspond to slightly lower conditions.
The magmatic cumulates crystallized at ca 0.6 GPa. The cumulate rocks evidence that the TTG parental magmas en route to the surface experienced fractional crystallization of a large amount of amphibole before crystallizing as tonalite–trondhjemite plutons at slightly shallower depths (ca 0.5 GPa).

1. Introduction

Archaean continental nuclei worldwide are made of sodic granitoids, i.e. tonalites, trondhjemites and minor granodiorites, that constitute the so-called TTGs. There is a broad consensus that TTGs originated by partial melting of hydrous metabasalts, namely garnet-bearing amphibolites, or sometimes eclogites, based on geochemical and experimental evidence (e.g. Jahn et al., 1981; Martin, 1987; Rapp and Watson, 1995; Clemens et al., 1996; Moyen and Stevens, 2006). However, examples of partially molten amphibolites are rare (Williams et al., 1995; Hartel and Pattison, 1996) and more often correspond to rocks much younger than Archaean in age (e.g. García-Casco et al., 2008). The scarcity of natural evidence limits the possibility to precise the P–T conditions of melting required for the formation of Archaean TTG magmas, and therefore to derive the corresponding thermal gradient, a necessary piece of evidence in the attempt to reconstruct the Archaean geodynamic setting. A large variety of Archaean metabasites, including migmatitic amphibolites, as well as amphibole-rich magmatic rocks, was exhumed in the Inyoni shear zone (ISZ) near Barberton. This unique collection provides the opportunity to investigate the reactions and P–T conditions for partial melting of amphibolites, as well as the differentiation processes that may have occurred in the TTG magmas en route to the surface.

2. Geological setting

2.1. Lithology and geochronology of the Barberton area

The well-known Barberton area contains the oldest rocks of the Archaean Kaapvaal province. It is made of the Barberton greenstone belt (3.55–3.21 Ga), surrounded by plutonic rocks intruded during

* Corresponding author. Tel.: +33 5 61 33 25 76; fax: +33 5 61 33 25 60.
E-mail address: anne.nedelec@get.obs-mip.fr (A. Nédélec).

three successive episodes (Fig. 1a). Protoliths of the greenstone belt are dominated by mafic to ultramafic volcanics at the base, with felsic volcanics and sediments becoming dominant at the top. The metamorphic grade is nowhere higher than greenschist facies conditions in the core of the greenstone belt. However, this metamorphism generally grades into a narrow amphibolite-facies rim near the contact with the plutons (Diener et al., 2005; Stevens and Moyen, 2007), although these contact amphibolites were never observed to have reached partial melting conditions so far. Three successive events of TTG intrusions (Moyen and Stevens, 2006) are represented respectively by the 3.51—3.55 Ga Steynsdorp pluton, the ca. 3.45 Ga trondhjemitic intrusions south of the belt (mostly the Stolzburg and Theespruit plutons), and the long-lived (3.29–3.21 Ga: Kisters et al., 2010) intrusion of the composite (leucodiorites to trondhjemites) Kaap Valley and Nelshoogte plutons, together with the Badplaas gneisses to the South-West of the belt. The 3.23 Ga (Kamo and Davis, 1994) Kaap Valley pluton is an homogeneous, nearly undeformed tonalitic to leucodioritic pluton (Robb et al., 1986). The Nelshoogte pluton is a composite sill complex (Belcher et al., 2005); its most typical component is a coarse-grained leucotrondhjemite, slightly older than the Kaap Valley pluton (3.24 Ga: De Ronde and Kamo, 2000), with smaller intrusions of an amphibole-bearing tonalite (similar to the Kaap Valley tonalite). The older trondhjemites are foliated, while the younger tonalites are essentially undeformed.

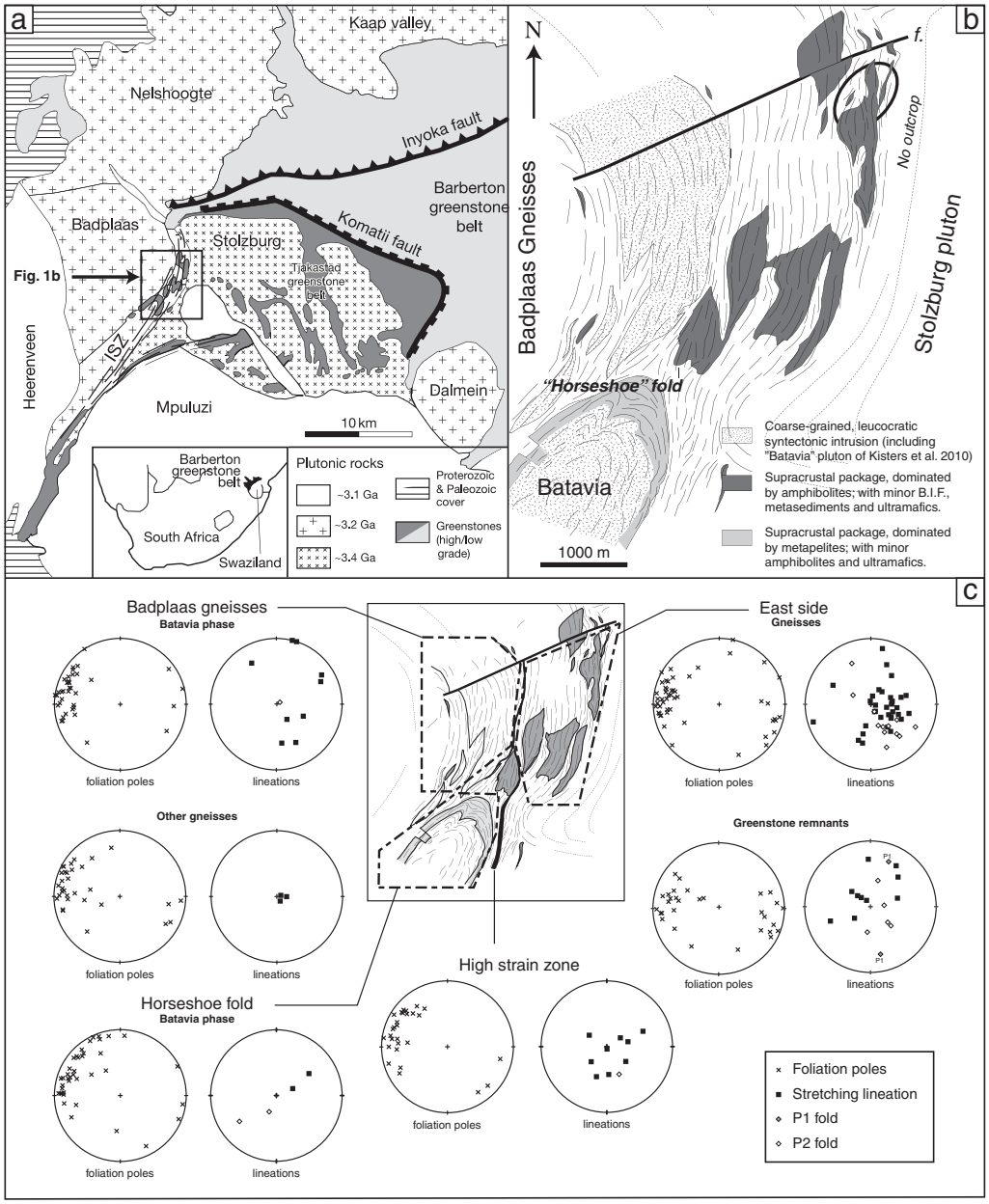

Fig. 1. (a) Geological map of the studied area, with location of the Inyoni shear zone (ISZ). (b) Detail map of the ISZ with location of the sampling area (circled). (c) Structural data from the ISZ area.

The Badplaas gneisses are somewhat older and shows a multitude of cross-cutting and variably deformed (but almost always foliated) tonalitic to trondhjemitic intrusions, ranging from 3.28 to 3.23 Ga (Kisters et al., 2010). A final set of intrusions is ca 3.1 Ga old; it is made of granites (e.g. Heerenveen granite: Belcher and Kisters, 2006) and granodiorites with subordinate syenites, and are therefore very distinct from the older TTGs.

2.2. Structural data

A major tectonic event occurred at 3.23–3.21 Ga and is regarded as the accretion of two different blocks along the Inyoka–Inyoni fault system striking NE–SW to NNE–SSW (Fig. 1a). The Inyoka fault is a major fault zone within the greenstone belt (Lowe, 1994; Lowe et al., 1999); it runs roughly ENE–WSW in the low-grade domain, and merges with the Komati fault (i.e. the major detachment separating the low-grade core of the belt from the high-grade rim (Kisters et al., 2003)). The Inyoni "shear zone" (ISZ) is the extension of the Inyoka fault in the high grade domain, south of the Komati fault. The ISZ is nearly 2 km wide and separates the (older) Stolzburg pluton from the (younger) Badplaas gneisses. The shear zone itself is made of variably deformed gneissic rocks, showing successive generations of syntectonic tonalitic veins or small intrusions intruding into each other. Some of these intrusions can be traced into the Badplaas gneisses. Countless supracrustal relics, whose sizes range from 1 m to 1 km, are found in the gneisses (Fig. 1b). This supracrustal package appears as a tectonic melange of metasediments and metabasites (Anhaeusser and Robb, 1980). All lithologies in the ISZ display a near-vertical, metamorphic or magmatic to solid-state foliation with typically steep stretching lineations, parallel to the fold axes, sometimes identified as sheath fold (Fig. 1c). Collectively, we interpret this strain pattern as reflecting vertical constriction along the edges of the emplacing Badplaas plutonic rocks, that were likely orthogneissified at that time. These structural data strongly suggest that the ISZ tectonic melange offers the unique opportunity to sample rocks exhumed from deeper levels than anywhere else in the greenstone belt. The 3..23 Ga age of a late-tectonic dyke (Dziggel et al., 2005) gives a minimum age for the last deformation stages in the ISZ, hence no younger that the latest Badplaas plutonic rocks (Kisters et al., 2010).

Older phases (3.28 to 3.25 Ga) of the Badplaas complex, found mostly in the West and South-West portions of the ISZ (e.g. the "Batavia pluton" in Kisters et al., 2010) show a preserved distinct structural pattern, dominated by less regular and somewhat shallower lineations and small-scale, both dextral and sinistral (conjugate) shear zones, that are commonly rotated into parallelism with the main foliation. As this pattern is restricted to the oldest components of the study area, we regard it as reflecting an older phase of dominantly E–W flattening.

The studied amphibole-rich rocks were all sampled in the ISZ. A few of the exhumed metabasites were already studied by Moyen et al. (2006), who focussed on the coldest and highest-pressure parageneses in these rocks. Their thermobarometric calculations yielded an apparent geothermal gradient of 12–15 °C/km for these HP rocks, that are partially retrogressed garnet- and CPx-bearing amphibolites. Here, we focussed on a different set of samples from the ISZ, including metamorphic and magmatic rocks (i.e. amphibolites and hornblendites), in order to get information on the genesis and evolution of the nearby emplacing TTG magmas.

3. Petrography

3.1. Metamorphic rocks

For the scope of this study, the most interesting samples are the migmatitic amphibolites. All samples were taken within 1 km in and around the large supracrustal remnant in the northern portion of the ISZ (unit SL1 of Dziggel et al., 2002), as shown in Fig. 1b. Garnet-bearing amphibolites displaying textures typical of in situ melting (INY134, .INY22 and INY25m) were carefully selected for detailed analytical work. They are heterogenous rocks, with a fine-grained mesosome and a large-grained neosome (following the terminology of Johannes, 1983), represented by a felsic leusosome (the former melt, that may have been partly segregated and locally fractionated, as frequently observed in migmatites: e.g. Taylor and Stevens, 2010) and various amounts of mafic minerals, newly formed and/or restitic, equilibrated with the melt. These mafic minerals either form well-defined layers or aggregates, or are evenly distributed in the leucosome. Injection migmatites, following the terminology of Mehnert (1968), i.e. rocks containing a leucosome formed elsewhere, may also be present and one sample (INY132) was selected to check this hypothesis. Two samples of non-migmatitic garnet-amphibolites (B34A1 and B34A2) were also retained, the first one (B34A1) being characterized by abundant large garnet crystals.

3.1.1. Migmatitic amphibolites

3.1.1.1. INY134. Mesosome and leucosome are easy to recognize (Fig. 2a). The mesosome is made of small (<100 μm) isogranular crystals of amphibole (70%), plagioclase (15%), quartz (15%) and accessory titanite. The leucosomes are ca 5 mm thick. They are locally underlined by a fine layer of large crystals of amphibole (1–2 mm in size) resembling a melanosomic selvage. The concentration of garnet crystals of a diameter lesser than 1 mm are recognized as newly-formed crystals, i.e. crystals belonging to a neosome (Fig. 2a). Large crystals of titanite, locally with an ilmenite core, are also present in this neosome. Rare unsegregated neosome garnet crystals are observed in the mesosome; they appear partly replaced by a peculiar type of amphibole, with larger grains than the typical mesosome amphibole. In the neosome, garnet is locally retrogressed to epidote.

3.1.1.2. INY25m. The mesosome displays a foliated texture and contains 50% amphibole, 35% quartz, 13% plagioclase and 2% titanite. Leucosome are made of large grains of quartz and plagioclase, and rare garnet (Fig. 2a). The garnet-rich neosome contains 55% garnet, 15% amphibole, 15% plagioclase and 15% quartz. Symplectitic coronae of epidote and quartz around a few garnet crystals are obviously the product of local retrogression of garnet in subsolidus conditions. A residua-enriched "mesosome" contains 70% amphibole, 15% feldspar (antiperthitic plagioclase: Fig. 2e), 10% epidote and 5% quartz. Accessory titanite is present everywhere.

3.1.1.3. INY22. A neosome ca 2 cm thick can be observed in this sample. It displays a granoblastic texture and contains 40% amphibole, 25% plagioclase, 25% quartz and 10% garnet. Garnet crystals are large (up to 5 mm in diameter) (Fig. 2a). They contain numerous titanite inclusions in their rims. Their outer rim also contains amphibole inclusions. No inclusion is observed in their core. Retrograde epidote after garnet is locally observed. A cumulative layer of (sub)automorphic amphibole crystals is also recognized in this sample.

3.1.1.4. INY132. This rock looks rather homogenous at the naked eye, but, in thin section (Fig. 2a), it was recognized as a migmatite, with an amphibole-rich neosome (zone 1) and an epidote-rich "mesosome" (zone 2). The leucosome is characterized by its larger grain size. It contains amphibole, plagioclase, quartz and accessory titanite. The epidote-rich mesosme contains amphibole, epidote, garnet, ilmenite and a few % alkali feldspar. This unusual mineral composition suggests that it may represent a restitic composition. This hypothesis will be checked by calculating zone 1 and zone 2 compositions (see below).

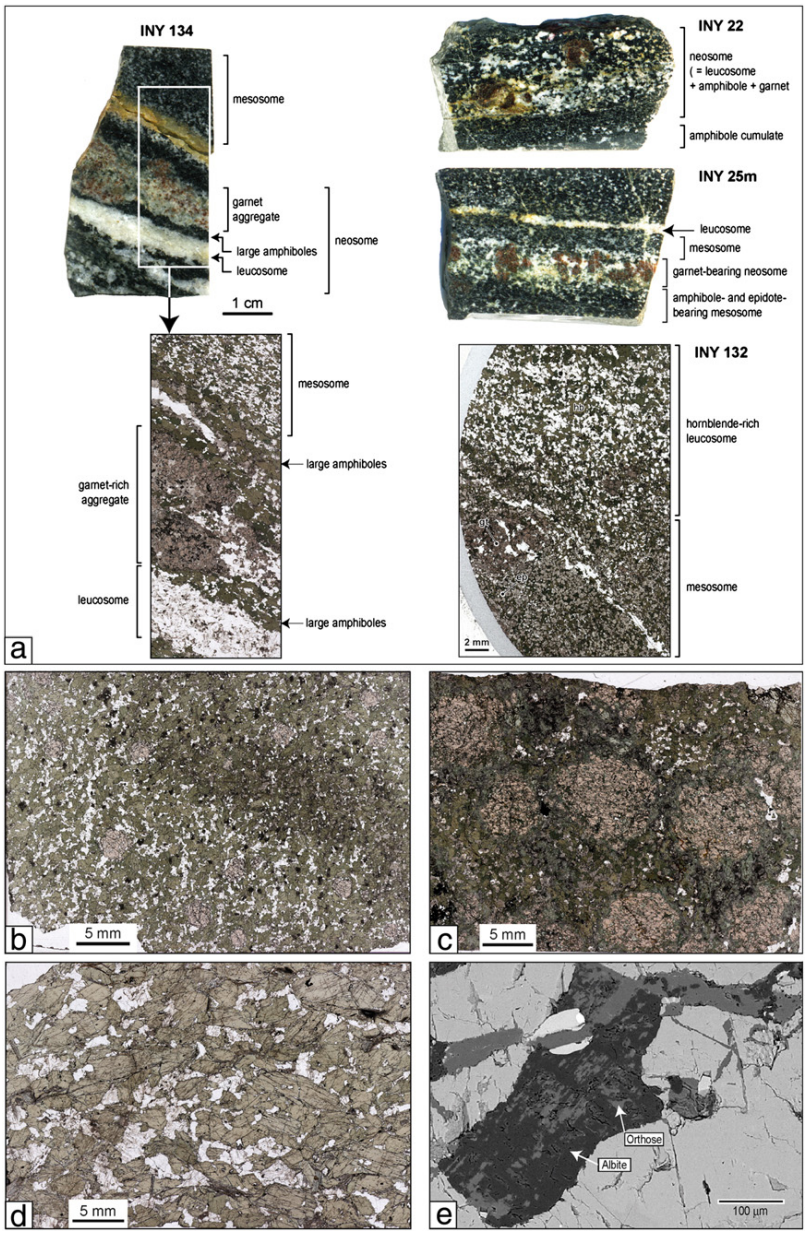

Fig. 2. (a): Migmatitic amphibolites: INY134 (with detailed microphotograph), INY25M, INY22 and INY132 (zone 1: hornblende-rich leucosome; zone 2: restite; zone 3: back-reaction zone) (b): non-migmatitic amphibolite B34A2; (c): restitic amphibolite B34A1; (d): hornblende-rich cumulate; (e): SEM image of antiperthitic feldspar in INY25m neosome.

3.1.2. Non-migmatitic amphibolites

3.1.2.1. B34A2. This rock has a homogeneous texture, with a fine-grained size (all grains <1 mm in diameter). It contains 65% amphibole, 20% quartz, 10% plagioclase, 5% garnet, accessory titanite and rare retrograde epidote after garnet. Garnet is distributed equally in the rock (Fig. 2b).

3.1.2.2. B34A1. This rock is characterized by abundant (60%) large garnet crystals (ca 5 mm in diameter: Fig. 2c) surrounded by a finer grained matrix of amphibole (20%), plagioclase (10%), clinopyroxene (5%) and quartz (5%). Symplectitic retrograde coronae of epidote and quartz are developed around the garnet prophyroblasts. The clinopyroxene is also partly replaced by a retrograde symplectitic association of epidote and amphibole. Accessory titanite and ilmenite are also present.

3.2. Magmatic rocks

Hornblende-rich cumulates (or hornblendites) are common in the metabasite package. They are locally crosscut by tonalitic to trondhjemitic dykes. The cumulates are characterized by their large (sub)automorphic amphibole phenocrysts, up to 1 cm in size (Fig. 2.d). The light minerals (plagioclase and quartz) display variable contents and crystallized later. When the light minerals are abundant, the rocks acquire a mushy texture. Apatite and allanite are the main accessory minerals. Three samples were selected for detailed study: INY6, INY20 and INY14. The last one appears to have acquired a greenschist facies overprint, responsible for the

Table 1
Representative amphibole compositions and structural formulae on the basis of 13 cations + (Ca, Na, K).

Rock type	Migmatitic amphibolites									Non-migmatitic amphibolites cumulates					Tonalite	
Sample no	INY134					INY25		INY132		B34A2	B34A1	INY6	INY20		B42	
	Mesosome		Neosome		Retrograde	Mesosome	Leucosome	Leucosome	Restite		Restite					
	Core	Rim	Core	Rim	After garnet			(Zone 1)	(Zone 2)				Core	Rim	Core	Rim
SiO_2	40.25	40.68	40.74	41.05	39.95	40.71	40.58	40.2	40.35	43.72	41.14	45.54	45.81	49.63	45.46	56.29
TiO_2	1.1	0.75	1.46	1.46	0.42	1.02	0.76	0.99	0.93	0.8	0.74	1.23	1.29	0.43	1.41	0
Al_2O_3	13.93	13.89	13.44	13.29	13.94	13.06	12.98	13.87	13.65	12.37	12.77	11.18	10.9	7.44	11.13	3.07
Cr_2O_3	0	0	0.06	0	0.03	0.07	0.01	0.02	0.05	0.14	0.05	0	0.19	0.02	0	0.13
Fe_2O_3 (c)	5.21	3.44	4.7	4.3	6.52	4.48	6.74	6.21	5.97	5.39	4.33	3.52	5.88	4.18	5.71	0
FeO (c)	16.64	17.81	16.03	16.69	18.47	17.35	16.73	16.06	17.61	12.7	18.47	9.95	7.4	8.29	10.16	11.77
MnO	0.1	0.15	0.38	0.24	0.43	0.31	0.35	0.34	0.24	0.16	0.21	0.43	0.24	0.07	0.34	0.12
MgO	6.5	6.29	7.11	7	4.65	6.42	6.41	6.6	5.6	9.5	6.03	12.03	13.26	14.78	10.93	14.4
NiO	0	0.11	0.03	0	0.08	0	0	0	0.06	0	0	0.02	0.07	0.04	0.12	0
CaO	11.49	11.61	11.2	11.51	11.32	11.34	11.73	11.6	11.37	11.66	11.52	11.61	11.32	12.14	11.17	12.01
Na_2O	1.18	1.35	1.64	1.31	1.31	1.41	1.19	1.28	1.2	1.36	1.2	1.29	1.62	0.89	1.05	0.29
K_2O	1.19	1.05	1.1	1.07	0.94	1.08	0.94	1.05	1.06	0.27	1.18	0.52	0.58	0.27	0.53	0.17
F	0	0.19	0	0.22	0	0	0	0	0	0.4	0.02	0.34	0.39	0.22	0	0
Cl	0.02	0	0	0.02	0.05	0	0.02	0.01	0.03	0.04	0.03	0.02	0	0.01	0.02	0.02
H_2O(c)	1.96	1.86	1.97	1.86	1.93	1.95	1.96	1.97	1.95	1.83	1.93	1.88	1.9	1.99	2.05	2.12
O = F	0	0.08	0	0.09	0	0	0	0	0	0.17	0.01	0.14	0.17	0.09	0	0
O = Cl	0	0	0	0	0.01	0	0.01	0	0.01	0.01	0.01	0.01	0	0	0.01	0
Sum ox%	99.57	99.09	99.88	99.91	100.03	99.21	100.41	100.19	100.06	100.17	99.62	99.43	100.69	100.3	100.07	100.4
Si	6.148	6.245	6.187	6.231	6.152	6.253	6.18	6.111	6.172	6.459	6.317	6.657	6.586	7.095	6.632	7.951
Ti	0.127	0.087	0.167	0.166	0.048	0.118	0.087	0.113	0.107	0.089	0.086	0.135	0.139	0.046	0.155	0
Al IV	1.852	1.755	1.813	1.769	1.848	1.747	1.82	1.889	1.828	1.541	1.683	1.343	1.414	0.905	1.368	0.049
Al VI	0.656	0.759	0.592	0.609	0.682	0.617	0.51	0.595	0.633	0.613	0.627	0.584	0.433	0.349	0.545	0.462
Cr	0	0	0.008	0	0.004	0.009	0.001	0.002	0.006	0.016	0.006	0	0.022	0.002	0	0.015
Fe3+	0.599	0.397	0.537	0.491	0.756	0.518	0.772	0.71	0.688	0.599	0.501	0.387	0.636	0.449	0.627	0
Fe2+	2.125	2.286	2.035	2.119	2.378	2.229	2.131	2.042	2.252	1.57	2.372	1.216	0.89	0.991	1.239	1.391
Mn2+	0.013	0.019	0.049	0.031	0.056	0.04	0.045	0.043	0.031	0.02	0.028	0.053	0.03	0.009	0.042	0.015
Mg	1.481	1.439	1.608	1.583	1.066	1.47	1.454	1.495	1.276	2.093	1.381	2.622	2.842	3.15	2.378	3.031
Ni	0	0.014	0.004	0	0.01	0	0	0	0.007	0	0	0.003	0.008	0.004	0.014	0
Ca	1.881	1.91	1.822	1.871	1.867	1.867	1.914	1.888	1.864	1.846	1.895	1.819	1.744	1.86	1.745	1.818
Na	0.35	0.401	0.484	0.386	0.391	0.421	0.352	0.376	0.355	0.39	0.357	0.367	0.45	0.246	0.297	0.08
K	0.232	0.205	0.214	0.207	0.185	0.212	0.183	0.203	0.206	0.052	0.231	0.098	0.106	0.048	0.098	0.031
F	0	0.09	0	0.108	0	0	0	0	0	0.186	0.011	0.157	0.179	0.101	0	0
Cl	0.004	0.001	0	0.004	0.013	0	0.006	0.004	0.009	0.009	0.008	0.006	0	0.002	0.006	0.005
OH	1.995	1.909	2	1.888	1.987	2	1.994	1.996	1.991	1.805	1.981	1.837	1.821	1.897	1.994	1.995
Sum cat#	17.463	17.516	17.52	17.464	17.443	17.501	17.449	17.467	17.424	17.288	17.483	17.283	17.3	17.154	17.141	16.841
XMg	0.411	0.386	0.441	0.428	0.31	0.397	0.406	0.423	0.362	0.571	0.368	0.683	0.761	0.761	0.657	0.685

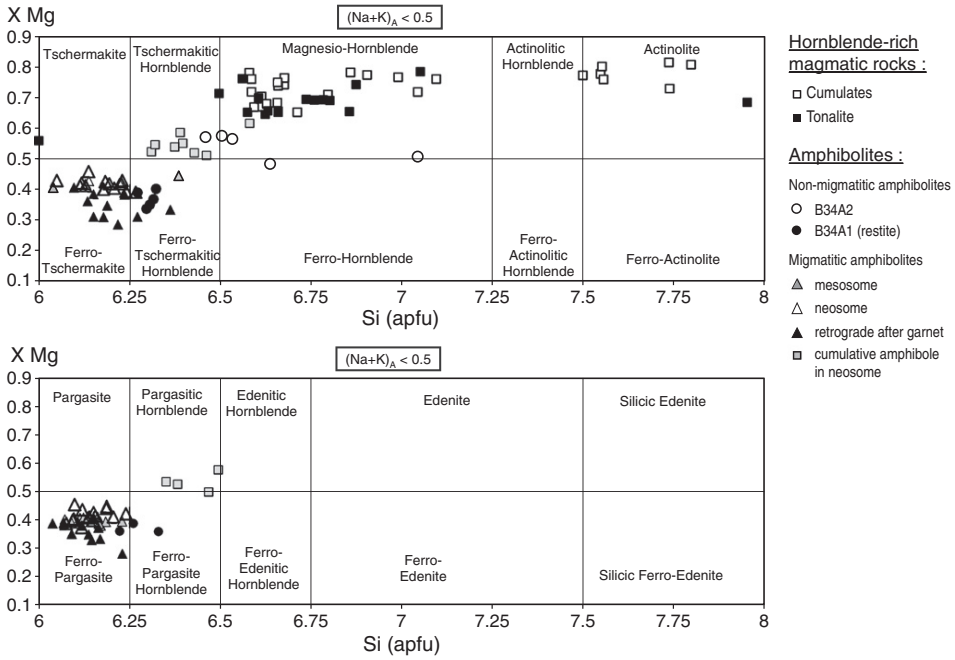

Fig. 3. Amphibole composition diagrams XMg vs Si (atom per formula unit: apfu) for $(Na+K)_A$ lower and higher than 0.5.

development of secondary epidote from plagioclase and for the growth of chlorite and actinote at the expense of amphibole. Finally, two plutonic rocks from the nearby Nelshoogte pluton were selected for comparison: a hornblende-rich tonalite (B42) and a trondhjemite NL-TMJ. They contain plagioclase, quartz, hornblende as the main minerals, and biotite and epidote as subordinate minerals. In numerous cases, epidote seems

Table 2
Representative garnet compositions and structural formulae on the basis of 8 cations.

Rock type	Migmatitic amphibolites						Non-migmatitic amphibolites			
Sample no	INY134		INY25		INY132		B34A2		B34A1	
									Restite	
	Core	Rim	Core	Rim			Core	Rim	Core	Rim
SiO_2	37.59	37.38	38.15	37.7	37.78	37.75	37.95	38.07	38.4	37.96
TiO_2	0.12	0.02	0	0.01	0.04	0.06	0.06	0.03	0.03	0
Al_2O_3	20.41	20.43	20.03	19.74	21.34	20.39	20.64	20.98	20.66	20.69
Cr_2O_3	0.03	0	0.02	0	0	0.11	0.05	0.05	0.03	0.07
Fe_2O_3 (c)	1.88	2.53	2.52	2.23	2.04	1.6	1.68	0.82	0.85	1.15
FeO (c)	22.08	21.47	21.02	20.79	22.23	23.85	21.75	24.26	22.86	22.79
MnO	2.81	2.63	2.59	2.33	2.08	2.09	2.78	1.59	0.94	0.72
MgO	1.41	1.64	1.51	1.5	1.65	1.72	2.18	2.32	0.92	1.14
NiO	13.75	13.79	15.06	15.05	13.99	12.62	13.26	12.13	16	15.49
CaO	100.08	99.88	100.9	99.35	101.15	100.18	100.34	100.23	100.68	100.01
Sum ox%										
Si	2.981	2.967	2.997	3.005	2.954	2.993	2.988	2.999	3.016	3
Ti	0.007	0.001	0	0.001	0.002	0.003	0.003	0.002	0.002	0
Al IV	0.019	0.033	0.003	0	0.046	0.007	0.012	0.001	0	0
Al VI	1.89	1.879	1.852	1.855	1.921	1.898	1.903	1.946	1.912	1.927
Cr	0.002	0	0.001	0	0	0.007	0.003	0.003	0.002	0.004
Fe3+	0.113	0.151	0.149	0.134	0.120	0.095	0.1	0.049	0.051	0.068
Fe2+	1.465	1.425	1.381	1.386	1.454	1.581	1.432	1.598	1.501	1.506
Mn2+	0.189	0.177	0.172	0.157	0.138	0.14	0.185	0.106	0.062	0.048
Mg	0.167	0.194	0.177	0.178	0.192	0.203	0.256	0.272	0.107	0.134
Ca	1.168	1.173	1.268	1.285	1.172	1.072	1.118	1.024	1.347	1.312
Sum cat#	8	8	8	8	8	8	8	8	8	8
XMg	0.102	0.12	0.114	0.114	0.117	0.114	0.152	0.146	0.067	0.082
Pyrope (%)	5.586	6.535	5.899	5.916	6.505	6.774	8.55	9.078	3.561	4.467
Almandin	49.014	48.008	46.067	46.112	49.170	52.77	47.876	53.269	49.749	50.202
Spessartine	6.309	5.947	5.741	5.222	4.671	4.68	6.19	3.527	2.067	1.61
Andradite	5.594	7.452	7.44	6.733	5.881	4.756	4.954	2.445	2.568	3.41
Grossulaire	33.402	32.058	34.801	36.008	33.765	30.662	32.262	31.533	41.962	40.094

to have crystallized, together with quartz, as a late-magmatic phase. However, in some cases, there is also secondary epidote developed after plagioclase.

4. Mineral chemistry

4.1. Analytical methods

All mineral compositions used for thermobarometry were obtained using the Cameca SX50 of the GET laboratory. Operating conditions were 15 kV and 20 or 10 nA (depending of the mineral strength, i.e. respectively for anhydrous and hydroxylated minerals), with a beam width of 1–5 μm. A few SEM observations were performed to determine the smaller phases.

4.2. Amphiboles

Representative compositions of amphibole are given in Table 1 and all data are plotted in the XMg vs Si (apfu) diagrams of Fig. 3. Amphibole from the plutonic rocks and from the cumulates are very similar. They are zoned crystals with a magnesio-hornblende core in the range $0.78 > XMg > 0.64$ and $6{,}25 < Si < 7$, and a less Al-rich composition toward the rim. Locally, an outermost rim of actinolite ($7{,}4 < Si < 8$) is also present and corresponds to a late reequilibration in greenschist facies conditions.

The metamorphic amphiboles are all richer in Al and Fe, and display ferro-tschermakitic to ferro-pargasitic compositions. Actually, two or three different compositions are recognized in the migmatites depending of the crystal location in the same sample (Fig. 3). Amphibole in the neosomes are slightly richer in Mg than amphiboles in the mesosomes, although these compositions are mostly overlapping and plot in the range $0.35 < XMg < 0.46$. The main contrast is observed in INY132, with amphibole XMg values in the range 0.41–0.49 in the neosome and 0.31–0.39 in the mesosome. Cumulative amphiboles in sample INY22 are also noticeably Mg-rich ($0.61 > XMg > 0.50$). In some samples, late retrograde amphiboles formed locally after garnet and display the less Mg-rich compositions ($0.34 > XMg > 0.27$). The non-migmatitic sample B34A2 has amphiboles rather rich in Mg. In the other amphibolite B34A1, amphiboles derived from the retrogression of the initial garnet-CPx assemblage are rather iron-rich.

4.3. Feldspars

Putting aside some albite-rich compositions in the outermost rims of some crystals, the composition ranges are generally narrow in all rocks, with the exception of the plutonic tonalite, where plagioclase displays a conspicuous normal zonation (An45-20) from a calcic core to a sodic rim. In migmatite INY134, plagioclase compositions are An35-30 in the mesosome and An31-27 in the neosome. The non-migmatitic plagioclase displays different compositions, with rather calcic plagioclase (An39-36) in B34A2 and more sodic ones (An32-22) in B34A1. Hornblende-rich cumulates INY6 and INY20 display restricted plagioclase compositions (An25-18). More sodic compositions in INY14 are explained by a stronger retrogression in greenschist facies conditions. Finally, a few alkali (K-Na) feldspars were analyzed in the neosome of INY134 and in the mesosome of INY132. Observations in SEM also revealed the antiperthitic nature of plagioclase in the INY134 migmatite and the INY25m neosome (Fig. 2e).

4.4. Garnets

Representative garnet compositions are given in Table 2 and all data are plotted in Fig. 4a. Garnets are all almandine-rich ($Fe/Fe + Mg + Ca \approx 0.50–0.63$). Their pyrope-contents are low ($Mg/Fe + Mg + Ca \approx 0.03–0.01$). The grossular-contents display the largest composition range ($Ca/Fe + Mg + Ca \approx 0.20–0.46$). The large garnet crystals of sample B34A1 are the more Ca-rich and the more Mg-poor, but they do not display any significant zonation, apart from a higher Mn-content in their core, that is typical of normal garnet growth in prograde conditions (Hollister, 1966). Only garnets from INY22 display a significant zonation, with a Ca- and Mg-richer rim (Fig. 4b), suggesting a prograde evolution toward higher P and T. The outermost rim with a reverse zoning is regarded as the result of a late exchange with nearby amphibole. In migmatites, garnet crystals are scarce or absent in the mesosomes. When they are present, they display the same compositions as garnets in the neosomes.

4.5. Epidotes

Epidote is present in most samples. In most cases, their pistachite content is in the range 21–26%. Actually, we use both composition and textural relationships to classify the epidotes. For instance, in

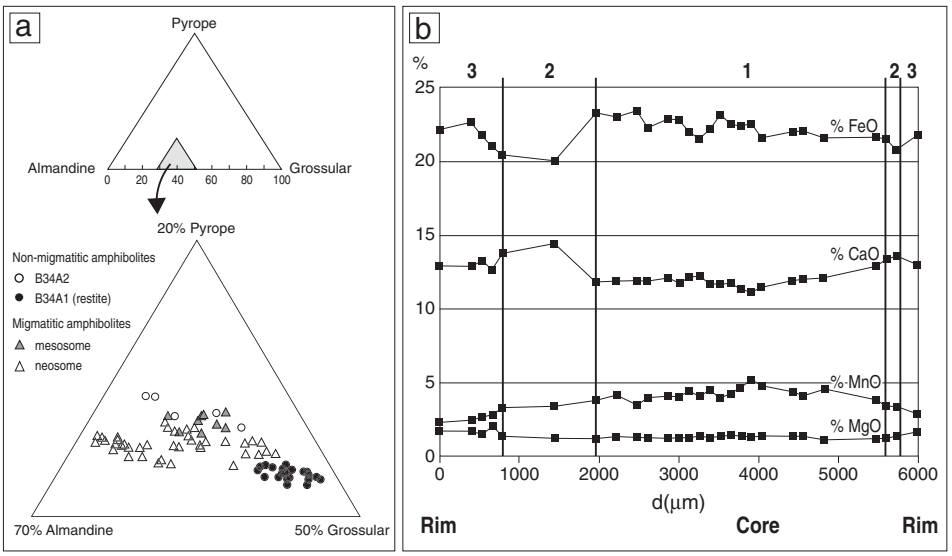

Fig. 4. (a) Garnet ternary composition diagram; symbols as in Fig. 3; (b) composition profiles in a large neosome garnet of migmatite INY22.

INY25m, a first generation of epidote (Ps = 21–23%) is present, whereas other epidotes, retrograde after garnet, have a higher Ps content (24–26%). The tonalite sample (B42) and some cumulate rocks (e.g. INY20) contain late-magmatic epidote (Ps = 22–25%) in interstitial position. In addition, some secondary epidote developed after plagioclase in the retrogressed cumulate INY14; it displays the lowest Ps content (Ps = 14–15%). These low pistachite contents are common in greenschist facies metamorphism (Grapes and Hoskin, 2004).

4.6. Pyroxene

Only B34A1 contains clinopyroxene either as inclusions in garnet or as matrix crystals in-between the large garnets. Both types display the same composition (0.53 > XMg > 0.42), at straddling the limit between the diopside and hedenbergite domains, and contain only 5% of jadeite.

5. Whole-rock chemistry

5.1. Analytical methods

Selected samples were analyzed in the Service d'Analyse des Roches et Minéraux (CRPG, Nancy). Grinded powders were melted with $LiBO_2$ and dissolved in HNO_3. Major elements were analyzed with ICP-AES and trace elements with ICP-MS, and results were checked by comparison with usual international standards. Detection limits are less than 0.1% (with an uncertainty of <2%) for major elements, and less than 1 ppm (with an uncertainty of <10%) for most trace elements.

Migmatites are heterogeneous rocks and, then, it would be useful to perform separate analyses of the mesosomes and of the leucosomes or neosomes. This was not an easy task and we succeeded only in separating and analyzing the mesosome of INY134. In the case of INY132, the respective proportions, i.e. areas, of the leucosome (zone 1) and of the

Table 3
Whole-rock compositions of selected samples.

Rock types	Non-migmatitic amphibolites		Migmatites				Hornblende-rich cumulates		Plutonic rocks	
					Calculated by image analysis					
Sample	B3 4A2	B34A1	INY134		INY132		INY 14	INY 20	B4 2	NL-TMJ
		Restite	Mesosome		"leucosome" (zone 1)	"mesosome" (zone 2)			Tonalite	Trondhjemite
SiO2 (%)	51.305	44.508	52.241		53.7	49.1	49.38	50.462	58.878	69.99
Al2O3	13.549	15.236	12.552		11.6	13.1	10.518	12.566	18.582	15.823
Fe2O3 tot	12.845	17.854	15.674		13.9	17.0	12.01	10.8	4.017	2.186
MnO	0.187	0.328	0.233		_	_	0.1865	0.112	0.052	0.0237
MgO	5.979	3.112	3.948		3.8	3.3	12.247	10.281	2.911	0.714
CaO	9.982	13.246	9.469		10.2	10.7	9.893	9.135	5.525	3.217
Na2O	2.337	1.317	2.137		1.8	1.3	1.535	2.373	4.979	5.302
K2O	0.368	0.628	0.744		0.6	0.9	1.04	0.754	1.868	1.082
TiO2	1.301	2.078	1.72		3.8	4.3	0.721	1.118	0.42	0.257
P2O5	0.177	0.286	0.279		–	–	0.06	0.042	0.164	0.1
PF	1.147	0.771	0.8		1.1	1.1	1.64	2.042	1.685	0.94
Total	99.178	99.365	99.797		100.0	100.0	99.22	99.684	99.08	99.63
Mg no	29	13	18		22	14	47	45	38	22
				Modal percentages						
Ba	24.27	80.39	25.01	Amphibole	58	40	99.95	79.7	148.7	147.3
Rb	16.72	24.02	7.311	Plagioclase	14	23.57	19.27	73.13	29.27	
Sr	164.3	174.1	81.12	Alkali feldspar		6	92.72	169.9	715.4	555
Co	47.05	83.34	96.7	Quartz	20	9	59.67	67.21	18.54	4.036
Cr	114.5	105.1	36.68	Epidote		19	1000	257.9	52.17	8.992
Ni	113.6	74.74	57.81	Garnet		20	304.4	226.8	48.1	8.615
V	357.3	421.5	485.8	Titanite	8		181.3	367.5	93.3	19.11
Nb	4.256	7.697	6.138	Ilmenite		7	3.338	3.303	1.26	1.852
Ta	0.331	0.565	0.495				0.405	0.497	0.126	0.189
Zr	96.94	145	114.4				41.93	41.92	45.81	122.3
Hf	2.537	3.728	2.934				1.533	1.589	1.301	3.018
Pb	1.2533	1.8133	1.7893				1.3466	3.022	3.0218	4.4985
Th	0.563	0.679	0.606				0.563	0.562	0.837	2.341
U	0.143	0.341	0.419				0.343	0.457	0.296	0.457
Y	31.54	48.13	38.29				16.18	13.31	6.67	2.924
Nb/Ta	12.9	13.6	12.4				8.2	6.6	10	9.8
La	7.471	8.834	6.513				4.988	4.518	7.074	18.97
Ce	17.51	23.84	17.58				17.87	16.46	15.75	33.11
Pr	2.759	3.544	2.669				2.956	2.318	1.943	3.665
Nd	12.96	17.53	13.08				13.6	11.16	8.396	12.68
Sm	3.822	5.566	4.15				3.586	3.325	2.097	1.786
Eu	1.358	1.883	1.459				1.179	1.133	0.823	0.608
Gd	4.656	6.873	5.286				3.38	3.408	1.854	1.04
Tb	0.823	1.241	0.951				0.512	0.492	0.257	0.121
Dy	5.298	8.149	6.228				2.993	2.686	1.346	0.567
Ho	1.107	1.708	1.323				0.565	0.487	0.236	0.097
Er	3.209	4.903	3.87				1.549	1.279	0.6	0.274
Tm	0.482	0.72	0.589				0.224	0.173	0.078	0.04
Yb	3.215	4.837	3.939				1.458	1.048	0.485	0.285
Lu	0.505	0.755	0.616				0.216	0.149	0.072	0.05
(La/Yb)N	1.6	1.2	1.1				2.3	2.9	9.8	44.9

restitic mesosome (zone 2) were determined by image analysis, giving 49% and 51% respectively. Next, modal composition of each zone was calculated according to the same image analysis for determination of the proportions of the mineral phases. Using the microprobe chemical composition of these minerals, we calculate a theoretical composition for each zone. The compositions of both zones are combined in their respective proportions to calculate a theoretical whole-rock composition to be compared with the analyzed whole-rock composition in order to check for the consistency of the method. The comparison between the measured and calculated whole-rock compositions yields a very good agreement ($r^2 = 0.97$), confirming the validity of the calculated leusome and mesome compositions.

5.2. Results

Whole-rock compositions are presented in Table 3. The non-migmatitic amphibolite B34A2 is very similar to typical Archaean tholeiites (Condie, 1981). Nevertheless, it is worth to notice that the other amphibolites display rather low mg numbers (mg# = 13–18). The sample B34A1 characterized by numerous large garnets has the lowest mg#, but the highest Fe_2O_3total + MgO (=21%), together with the lowest SiO_2 and the highest Al_2O_3, TiO_2 and CaO contents, suggesting a restitic nature. The alternative hypothesis that it could represent a metamorphosed ferrobasalt is not retained, because CaO is too high and SiO_2 is too low with respect to typical ferrobasaltic compositions (Namur et al., 2010). Compared with the other garnet amphibolite (B34A2), it also displays a lesser amount of Cr and Ni, but a higher amount of Co, V and high field strength elements (HFSE), i.e. Nb, Ta, Zr, Hf , Th, U and Y, in agreement with a greater content in accessory phases such as Fe-Ti oxides and zircon. Actually, the INY134 mesosome may also have been slightly enriched in restite component due to its intermediate composition, and its mg# and trace element contents. These samples (B34A1, B34A2 and INY134) have nearly flat REE distribution patterns (Fig. 5), like most Archaean tholeiites; B34A1 has the highest REE content.

The hornblende-rich cumulates display mafic compositions, with mg# higher than in the amphibolites, together with rather high Fe_2O_3total + MgO (=19–22%). However, they have lower MnO, TiO_2 and P_2O_5 contents. Their very high Cr and Ni contents are consistent with their cumulative nature, both elements being present in the hornblende as shown by Table 1. The HFS elements display lower contents than in the other amphibolites. Their REE distribution patterns are fractioned, as a consequence of their lower HREE contents, hence rather similar with the REE patterns of typical TTGs (Fig. 5). Their La contents display a small negative anomaly.

The analyzed TTs were selected as representative end-members of the nearby plutons, that is from a hornblende-rich tonalite to a trondhjemite composition. They are typical of Archaean TTGs, with K_2O/ Na_2O = 0.2–0.3, low Fe_2O_3total + MgO, fractionated REE distribution patterns and low to very low HREE contents (Fig. 5). In the Sr vs SiO_2 diagram of Moyen (2011), they plot in the field of medium-pressure TTGs, that represent some 60% of the TTG database. Differences between the cumulative hornblendites and the tonalite are consistent with lower amounts of modal amphibole (magnesiohornblende) and titanite, and higher amounts of plagioclase and quartz in the tonalite. Hence, these rocks can be regarded as related by a fractional crystallization process. Besides, the low (<15) Nb/Ta ratios are conspicous and will be discussed later.

6. Thermobarometry

6.1. Methods

Various methods were used depending of the lithologies. The hornblende-garnet thermometer of Graham and Powell (1984) can be used for hornblende and garnet, that were in equilibrium in migmatitic as well as non-migmatitic amphibolites. However, these minerals may have been submitted to some retrograde Fe-Mg exchange during cooling and decompression, as demonstrated by outermost rims with slightly lower CaO and higher FeO in the INY 22 neosome garnets for instance (Fig. 4b). Therefore, calculated temperatures may be only minimal values with respect to peak temperatures. On the other hand, temperature calculations in excess of 850 °C are usually dismissed, as less reliable, following the advice of Graham and Powell (1984). The semi-quantitative thermobarometer of Ernst and Liu (1998) can also be used in the same metabasites, at least in a comparative way. It is based on the Al_2O_3 and TiO_2 contents in the amphibole. P and T are determined graphically. TiO_2 isopleths are only temperature-dependent and their intersections with Al_2O_3 isopleths provide a pressure estimate. This thermobarometer must be used with caution, because Ti is often exsolved as titanite or ilmenite during slow cooling of amphibole, hence a T estimate that will be too low and, consequently, a P estimate that will be too high. Therefore, the most reliable estimates are those obtained with amphibole

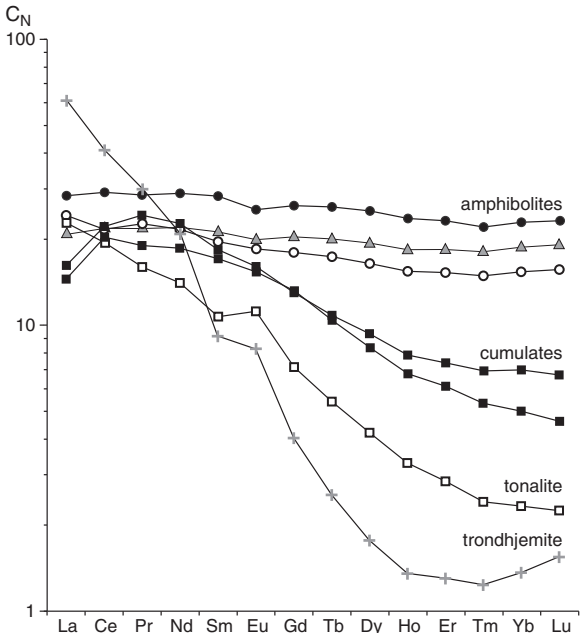

Fig. 5. REE distribution patterns; symbols as in Fig. 3.

Table 4
Endmembers used for pseudosection calculation (see documentation in Perple_X-07 for references on solid solution models – http://www.perplex.ethz.ch).

Mineral	Solid solution model	Endmembers
Chlorite	Chl(HP)	daph, ames, afchl, clin
Clinopyroxene	Omph(GHP)	di, jd, acm, hed
Amphibole	Amph(DPW)	tr ftr parg fparg_i ts fts_i gl fgl_i
Biotite	TiBio(WPH)	ffbi_i fbi ftbi_i tbi1 sdph_i east ann phl
Epidote	Ep(HP)	cz fep
Garnet	Gt(WPH)	spss alm py gr fmn_i fkho_i kho_i andr
Ilmenite	IlHm(A)	ilm hem mfets ffets_i
Phengite	Pheng(HP)	pa, cel, fcel, mu
Paragonite	MuPa	mu, pa
Cordierite	hCrd	fcrd, crd, hcrd
Plagioclase	Pl(h)	abh, an
K-feldspar	Kf	mic, ab
Melt	Melt(HP)	h2oL, fo8L, fa8L, abL sil8L, anL, kspL, q8L

analyses displaying the highest Ti contents. Hence, the highest T and the lowest P are retained (see Table 5).

Pressure estimates can be obtained in the magmatic rocks (cumulates, tonalite, trondhjemite) from Al-in-hornblende barometry using the calibration of Schmidt (1992), that was established for tonalitic compositions containing quartz, feldspar (plagioclase), hornblende, biotite, epidote and accessories, and are near to saturation in orthoclase. The barometer is appropriate for rocks of calc-alkaline bulk magmatic compositions, that fill the requested conditions of mineral assemblage and fO_2 as can be deduced from the presence of epidote or magnetite and from a high enough XMg in amphiboles. In addition, rim magmatic hornblende compositions were used as recommended, because they correspond to crystallization temperatures immediately above the solidus, i.e. corresponding to the calibration.

P–T pseudosections display the univariant reactions and multivariant mineral assemblages that are encountered by a particular rock composition (Proyer, 2003). They are suitable for determining proportions and composition of a mineral assemblage during metamorphic peak condition and where equilibrium can be assumed. Pseudosections are inappropriate (in theory) for assessing changing mineral parageneses in rock types that preserve relic metamorphic assemblages or zoned minerals as garnet (Le Bayon et al., 2006), or that are characterized by an inhomogeneous distributions of mineral assemblages.

The pseudosection approach in the high-grade Barberton terrain is restricted, because some rocks recorded a multi-stage metamorphic evolution (Moyen et al., 2006) or are heterogeneous (e.g. INY132), and others may have loss a melt-component (e.g. B34A1). Other limitations are due to the absence of appropriate melt model for metabasic systems (Pitra et al., 2010), to the quality of the selected thermodynamic properties of minerals end-members and those of their mixtures as amphiboles and pyroxenes or to the H_2O activity and fluid saturation condition in our models.

As a whole, we have considered that the most suitable samples for this approach are the non-migmatitic amphibolite B34A2, and the migmatitic amphibolite INY134, assuming that both rocks did not loss a significant volume of melt. The pseudosections were constructed for conditions between T = 400–1100 °C and P = 1–15 kbar, to model the P–T range indicated by the thermobarometry. They are presented using a MnTiCaNKFMAS ($MnO–TiO_2–CaO–Na_2O–K_2O–FeO–MgO–Al_2O_3–SiO_2$) grid and for H_2O saturation conditions corresponding to the loss on ignition given by the whole rock analyses. We used version 2007 of Perple-X and the internally consistent thermodynamic dataset termed solut_09.dat available at www.perplex.ethz.ch/. The phases considered in the pseudosection calculations and references to the activity–composition models used are given in Table 4.

6.2. Results of classical thermobarometry

Results are presented in Table 5. Garnet-hornblende thermometry yield average neosome temperatures of 773 °C (721–823 °C) for INY134, 800 °C (773–817 °C) for INY 25 m, 747 °C (716–807 °C) for INY22 and 732 °C (706–745 °C) for INY132. All these results suggest that melting occurred at temperatures comprised between 730 and 800 °C. The garnet core compositions in sample INY134 yields a slightly lower temperatures of 701 °C, possibly corresponding to a pre-melting stage. The non-migmatitic and non-restitic garnet-amphibolite B34A2 yields a consistently lower temperature of ca 686 °C. By contrast, the restitic garnet-amphibolite B34A1 yields a somewhat higher temperature of 763 °C (754–772 °C). At last, the late iron-rich amphiboles formed after late garnet-retrogression yields a lower temperature of 684 °C (642–730 °C).

Using the highest Ti-contents values of the amphiboles, the Ernst and Liu (1998) thermobarometer provides T estimates of 730–790 °C and P estimates of 11.5–12.5 kbar for the migmatitic and restitic amphibolites. The non-migmatitic amphibolite B34A2 yields slightly lower conditions : T ≈ 730 °C and P ≈ 11 kbar. Despite some high P estimates (> 13 kbar) that have to be questioned because of the absence of rutile in the studied rocks, this barometer display consistent respective conditions for the different samples.

Al-in-hornblende barometry was used for amphiboles, that were in equilibrium with a tonalitic (*s.l.*) melt, i.e. the hornblende-rich cumulates and the Nelshoogte tonalite. The calculations suggest that the cumulates crystallized between 5.1 and 6.6 kbar, in mid-crustal conditions. The tonalite crystallized at 4.4–5.2 kbar, i.e. possibly in

Table 5
P, T estimates.

			Graham & Powell 1984	Ernst & Liu 1998	Schmidt 1992	Perple-X
			(Averages in bold)	(Preferred T and P in bold — see text)	(Averages in bold)	
Migmatites						
INY134	Mesosome	T (°C)		**750** (720–750)		**680** (650–710)
		P (kbar)		**14** (15–14)		**10.8** (9.4–11.5)
	Neosome	T (°C)	**773** (721–823)	**790** (720–790)		
		P (kbar)		**12.5** (15–12.5)		
	Late-retrogression	T (°C)	**684** (642–730)			
INY25m	Mesosome	T (°C)	–	**735** (670–735)		
		P (kbar)		**11.5** (14–11.5)		
	Neosome	T (°C)	**800** (773–817)	**760** (690–760)		
		P (kbar)		**12** (13–12)		
INY22			(Garnet core –zone 1): **701** (Garnet rim – zone 2): **747** (716–807)			
	Neosome	T (°C)		**760** (690–760)		
		P (kbar)		**12** (13–12)		
INY132	Neosome	T (°C)	**732** (706–745)	**720**		
		P (kbar)		**15**		
Garnet-amphibolites						
B34A1	Restite	T (°C)	**763** (754–772)	**730** (680–730)		
				12.5 (16–12.5)		
B34A2	Unmelted	T (°C)	**686** (685–687)	**730**		**650** (600–700)
		P (kbar)		**11**		**9** (8–10)
Cumulates						
INY6		P (kbar)			**5.9** (5.1–6.6)	
INY20					**5.8** (5.2–6.3	
INY26					**6.2**	
TTG pluton						
B42	Tonalite	P (kbar)			**4.8** (4.4–5.2)	

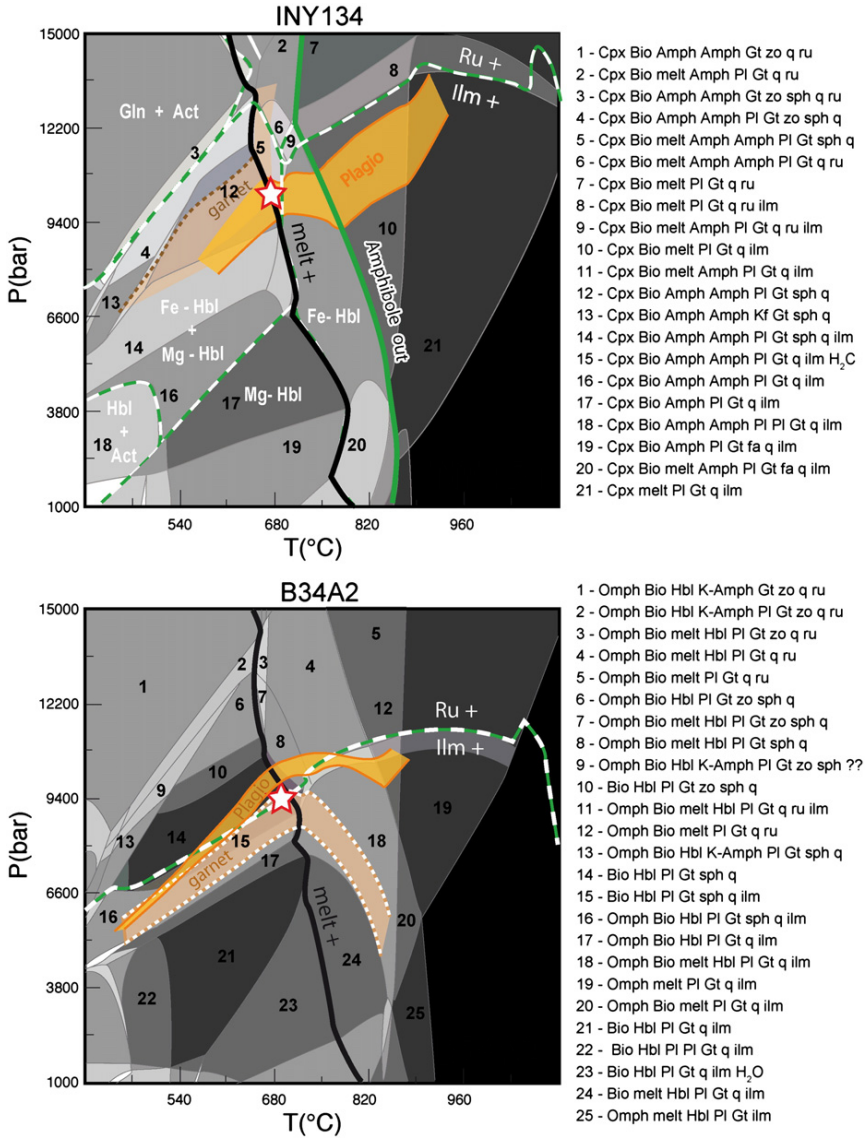

Fig. 6. PerpleX pseudosections for INY134 and B34A2.

slightly shallower conditions, but still consistent with the lower pressure limit of magmatic epidote (5 kbar) after Schmidt and Thompson (1996).

6.3. Results of P–T modelling

Stable assemblages in pseudosections were calculated for the non-migmatitic amphibole B34A2 and the migmatite INY 134 (Fig. 6). The pseudosection build for sample INY134 is given in Fig. 6A. In the grid, all the mineral assemblages at subsolidus conditions (T > to 600–800 °C) contain H_2O, whereas all the mineral assemblages at suprasolidus conditions contain a melt phase. Close to the subsolidus conditions and in the absence of rutile, the observed mineral assemblage garnet-plagioclase-amphibole-biotite is stable over a large pressure range, from 9 to 13 kbar. Perple-X modelling on the mineral compositions of chemically-zoned garnets (FeO/MnO ratio) growing in equilibrium with plagioclase (CaO/CaO + Na_2O ratio) and amphibole (FeO/FeO + MgO ratio) leads to refine the melting condition for this sample at P = 10–11 kbar and T = 650–700 °C (red star in Fig. 6A).

The pseudosection build for sample B34A2 is given in Fig. 6B. The observed mineral assemblage garnet-plagioclase-amphibole–titanite, with the absence of pyroxene and melt is stable over a large pressure range, from 7 to 11 kbar. Perple-X modelling on the mineral compositions of chemically-zoned garnets (FeO/MnO ratio) growing in equilibrium with plagioclase (CaO/CaO + Na_2O ratio) leads to refine the peak P–T conditions for this sample at 9–10 kbar and 650–700 °C (red star in Fig. 6B).

P and T estimates are lower than in classical thermobarometry. They are ca 680 °C and 9.5 kbar for B34A2 and 700 °C and 10.5 kbar for INY134. The latter values are obtained by considering that INY134 just crossed its solidus, but T conditions (if not P) may have been slightly higher, depending of the melting degree. Indeed, the absence of rutile strongly constrains the P conditions and the determination of the rutile-in curve is one of the most important results in the modelling approach. At P ≈ 10 kbar, the solidus has a negative slope and is no higher than 700 °C in our model. It is also worth to notice that the natural assemblages do not show any pyroxene (with the sole exception of the restitic sample B34A1), but sometimes contain primary epidote, whereas the calculated assemblages at P ≈ 10 kbar and 700 °C contain pyroxene, but no epidote. Further work would

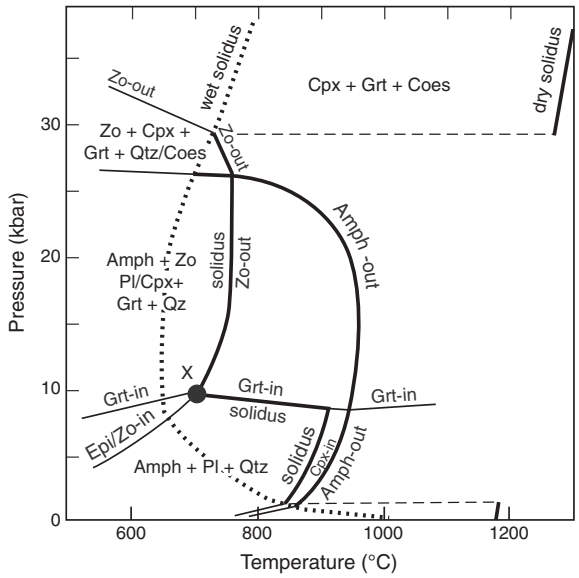

Fig. 7. P–T diagram of Vielzeuf and Schmidt (2001) compiling all possible melting reactions in a quartz-saturated (tholeiitic) metabasalt.

thus be necessary to strengthen the quality of our grids and the reliability of our P–T estimates, especially regarding the determination of H_2O activity, $f(O_2)$ and fluid saturation condition in our models

7. Discussion

7.1. The amphibolite melting reaction

Petrographic observations and mineral and whole-rock chemistry point to a partial melting reaction of the garnet-amphibolites producing a tonalitic (or trondhjemitic) liquid in equilibrium with garnet, amphibole and titanite (±clinopyroxene, ±epidote). Actually, there is a progressive compositional change in the amphibole towards higher XMg during melting, and at the same time, and increase in the garnet amount abundance, hence a low mg# in restitic, or restite-enriched, rocks. Epidote is often present either as a primary phase (e.g. INY 132) or as a secondary phase formed after garnet, possibly as a product of some back-reaction between melt and garnet. Comparing the observed mineral assemblages and P–T estimates with the metabasalt melting reactions revisited by Vielzeuf and Schmidt (2001), our samples would have experienced conditions close to point X in Fig. 7, thus partial melting at the amphibole-out curve is excluded, because it requires much higher T and/or P, and production of an anhydrous eclogitic or granulitic restite. Nevertheless, partial melting might have occurred through three different reactions, namely at the wet solidus, at the epidote-out solidus or even at the garnet-in solidus.

Epidote is not present in this last reaction, whereas it seems to play a role in most samples either as a reactant mineral of the prograde melting reaction or as a product of some back-reaction between garnet and melt. Hence, this reaction may have occurred in migmatites containing plagioclase, but no epidote in their mesosome, such as INY134. However, it would have been more consistent with a somewhat higher geothermal gradient (Fig. 8).

Fluid-present melting may occur at temperatures as low as 650 °C at $P \geq 8$ kbar. However, the unmelted sample B34A2 experienced higher conditions without melting. On the other hand, the presence of a fluid phase during prograde metamorphism remains highly speculative. This hypothesis is retained by some authors dealing with cases of slab melting (e.g. García-Casco et al., 2008). A fluid phase may be produced by the crystallization of a water-saturated melt, for instance a TTG melt produced at depth. However, such a melt is likely to be water-undersaturated at pressures around 10 kbar, and the cumulate evidence shows that the TTG melts likely ascended up to shallower levels before beginning to crystallize.

At last, the epidote-out solidus appears as the most likely and the corresponding reaction would have been :

$$\text{amphibole 1} + \text{epidote} + \text{quartz} + \text{plagioclase} \pm \text{garnet 1} = \text{liquid} + \text{amphibole 2} + \text{garnet 2} \pm \text{CPx}$$

Depending of the first exhausted phase, the mesosome would have evolved towards more refractory modal compositions, either devoid of epidote (INY134) or plagioclase and/or quartz (INY25m, INY132). Meanwhile, the amphibole composition becomes more magnesium-rich and the abundance of garnet increases. Indeed, some of the so-called mesosomes may have been modified by various degrees of partial melting. Garnet-amphibolites with very low mg# such as B34A1 may be

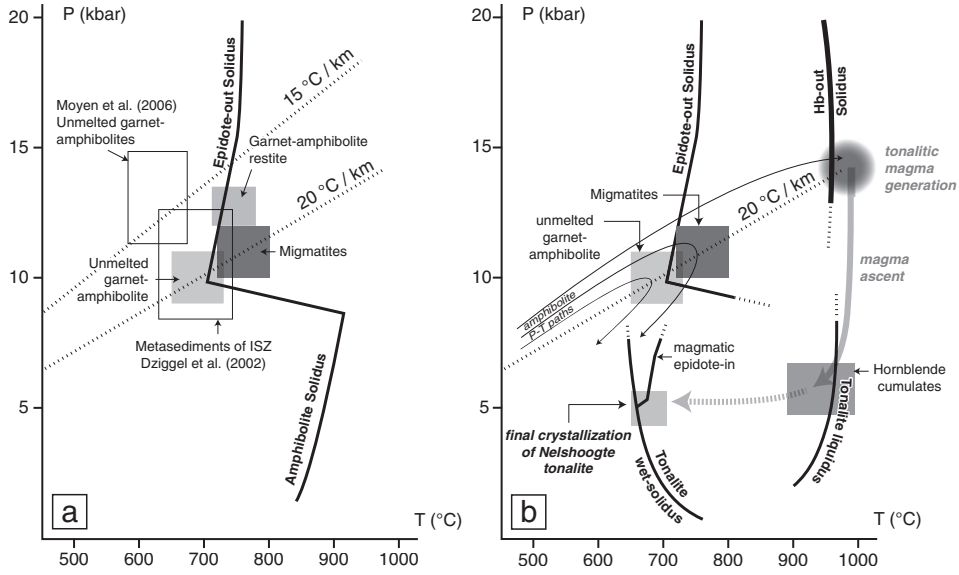

Fig. 8. (a) P–T diagram with compilation of thermobarometric results and geothermal gradients; amphibolite solidus after Vielzeuf and Schmidt (2001). (b) P–T paths for rocks and melts; tonalite liquidus after Prouteau and Scaillet (2003), and tonalite solidus and magmatic epidote stability after Schmidt and Thompson (1996).

Please cite this article as: Nédélec, A., et al., TTGs in the making: Natural evidence from Inyoni shear zone (Barberton, South Africa), Lithos (2012), doi:10.1016/j.lithos.2012.05.029

originally iron-rich rocks and/or secondarily iron-enriched rocks after the segregation and escape of a tonalitic melt, also dragging away some of the newly formed Mg-rich amphiboles.

7.2. The geothermal gradient

The thermobarometric estimates obtained from the studied samples are plotted in Fig. 8a, together with the epidote-out solidus of Vielzeuf and Schmidt (2001). The P–T conditions for the unmelted amphibolites (T = 650–730 °C; P = 0.9–1.1 GPa) are slightly lower than for the other samples, and plot just below the solidus. Taken together, the migmatitic and restitic amphibolites registered temperatures in the range 720–800 °C and P conditions in the range 1.1–1.2 GPa The corresponding geothermal gradient would have been in the range 17–22 °C/km. Moyen et al. (2006) obtained temperatures of 600–650 °C and pressures of 1.2 to 1.5 GPa in unmelted metabasites from the ISZ, hence a geothermal gradient of ca 12–15 °C/km (a value typical of subduction environments), that is the lowest metamorphic field gradient documented so far for the Archaean. This result is not at odds with the present thermobarometric estimations, as the studied samples are different and may represent different portions of the lower crust and/or different snapshots of the geological history, that finally culminated in the building of the 3.2 Ga plutons. On the other hand, our calculations are in close agreement with the values deduced from ISZ metasediments by Dziggel et al. (2002).

Regarding the formation of voluminous TTG melts, it was necessary to reach higher temperatures, i.e. to reach the amphibole-out reaction (Fig. 8b), but still to remain in the rutile-free domain, because of the analyzed Nb/Ta ratios in the plutonic rocks. Indeed, rutile would favor Ta with respect to Nb when coexisting with a melt (Xiong et al., 2005), yielding TT liquids characterized by higher Nb/Ta ratios that are not observed here. Therefore, TTG parental magmas should derive from melting of an amphibolitic and not a rutile-bearing eclogitic protolith (Foley et al., 2002). Taking into account the rutile-in curves in Fig. 6, the pressures could not have been much higher than 13.5 kbar, corresponding to T of ca 950 °C with the calculated gradient. Liquids with high mg# are expected in these temperature conditions (Wolf and Wyllie, 1993). These conditions are in agreement with the geothermal gradients that might have corresponded to the formation of medium-pressure TTGs after Moyen (2011). Indeed, Moyen (2011) described three groups of TTGs (high-, medium- and low-pressure) and concluded that each group formed along a distinctive geothermal gradient. The medium-pressure group was proposed to form roughly along the same geotherm as the one determined in this paper. In other words, our study provides a piece of evidence for the origin of this medium-pressure group.

Nevertheless, the tectonic environment at the time of TTG magmas formation remains poorly constrained. Moyen et al. (2006) speculated that partial melting of the ISZ amphibolites occurred during the decompression part of the P–T-path. Our study found no high pressure relics in the migmatitic amphibolites and found no sign of decompression melting. Therefore, we suggest that partial melting occurred during a prograde path, before their exhumation. This requires that the metamorphosed equivalents of hydrated basalts can arrive at depths of ca 50–55 km by some dynamic process (subduction, sagduction or whatever…). Nevertheless, all studied samples, whether partially molten or not, collectively represent an exhumed tectonic melange possibly corresponding to different P–T-paths (Fig. 8b).

7.3. Evolution of the TTG melts during segregation and ascent

Medium-pressure TTG melts are likely to be rather tonalitic in composition (Moyen, 2011). It was difficult to determine the composition of the leucosomes in the studied samples. Moreover, the leucosomes may not represent the original melt composition. The calculation attempted for INY132 yielded a quartz-dioritic composition (see Table 3). Actually, leucosomes or neosomes often display a more or less pronounced enrichment in mafic phases, such as Mg-amphibole, garnet and/or titanite, suggesting the loss of a felsic liquid component, hence implying an efficient segregation process even at low degrees of melting. Indeed, Wolf and Wyllie (1995) experimentally found that melt formed in amphibolites may segregate very easily in dynamic conditions, even at very low degrees of melting. The segregation process is favored by the intrinsic anisotropy of amphibole-rich rocks and possibly also by a rather low viscosity of the TTG melts.

None of the studied migmatites can explain the formation of large volumes of TTG magmas, that likely occurred at higher P and T due to the amphibole-out melting reaction (Fig. 8b). This requires that the metamorphosed equivalents of hydrated basalts arrived at the corresponding depths (50–55 km) by some dynamic process (subduction, sagduction or whatever…). The hornblende-rich cumulates derived from these HP–HT melts. Their crystallization at shallower depths constrain the melt ascent path, that should have been rather steep before crossing the tonalite liquidus, where amphibole crystallized and ascent was delayed due to the high crystalline charge (Fig. 8b).

A crystal fractionation process occurred in these mid-crustal conditions (ca 5 kbar). High XMg-hornblende is the main fractionating phase after thin section observations. This point was checked by a mass-balance calculation based on the 8 major oxides (neglecting MnO and P_2O_5, and with total iron as FeO) using the Petrograph software of Petrelli et al. (2005), based on the XLFRAC model of Stormer and Nicholls (1978). Indeed, using INY20 as a supposed parental composition, it is possible to obtain the tonalite composition (B42) after ca 68% of crystal fractionation of a cumulate containing only hornblende (with the composition of the INY20 amphibole core). No plagioclase appears in the cumulate calculation, confirming that hornblende is the main liquidus phase. This is in agreement with the experiments of Prouteau and Scaillet (2003), provided that the TTG parental melts were rich enough in water (H_2O wt% ≥ 7% at 500–600 MPa). Later, fractional crystallization of the tonalite magma involving amphibole and plagioclase would yield some more evolved trondhjemitic composition, such as NL-TMJ. Calculation of the corresponding cumulate yields 35% magnesio-hornblende, 64% plagioclase An44 (the core composition of plagioclase in the tonalite) and 1% accessories. This later process cannot be responsible for the formation of the studied hornblende-rich cumulates of the Inyoni shear zone, because they do not contain cumulus plagioclase. The studied cumulates correspond to an earlier fractionation stage in the TTG parental melt.

All the amphibole-rich cumulates record very similar pressure conditions, pointing to the existence of a specific level in the crust, corresponding to a depth of ca 17 km, where most of the TTG magmas were stopped. This depth may correspond to a lithological and/or a rheological transition (the ductile-brittle transition) in the crust. The residual melts crystallized only slightly higher, as confirmed by the presence of late-magmatic epidote, whose stability domain is higher than 5 kbar after Schmidt and Thompson (1996). Despite the scarcity of barometric data, the determined emplacement levels seem to be usual for Archean TTG plutons (e.g. Dziggel et al., 2002; Beakhouse et al., 2011).

8. Conclusions

Amphibole-rich rocks exhumed in the Iniony shear zone at the time of the emplacement of the 3.2 Ga Nelshoogte–Badplaas tonalitic to trondhjemitic plutons belong to two different groups. Some of them are garnet-amphibolites, displaying different degrees of partial melting. Unmelted garnet-amphibolites have a typical tholeiitic composition, whereas the migmatitic amphibolites become more iron-rich with melting. Restitic compositions are characterized by low-silica contents and low mg#, together with an enrichment in some trace elements (Co, V, HFSE). The melting reaction likely occurred at the epidote-out solidus and corresponds to P–T conditions in the range 11–12 kbar and 720–800 °C, hence a geothermal gradient of 17–22 °C/km, consistent with the genesis of medium-pressure TTG

plutons. The migmatitic amphibolites likely experienced the loss of a felsic liquid component. However, formation of large volumes of tonalitic magmas likely occurred at deeper conditions by crossing the amphibole-out melting reaction. The hornblende-rich cumulates (or hornblendites) crystallized in the middle crust at ca 6 kbar from TTG parental melts formed at deeper conditions, hence their higher mg#. Emplacement and final crystallization of the tonalitic to trondhjemitic plutons occurred at slighly shallower levels (ca 5 kbar).

Acknowledgments

C. Cavaré, S. Gouy, J.F. Mena, F. and P. de Parceval are warmly thanked for the technical assistance. Reviews by A. García-Casco and an anonymous reviewer contributed to improve the manuscript.

References

Anhaeusser, C.R., Robb, L.J., 1980. Regional and detailed field and geochemical studies of Archaean trondhjemitic gneisses, migmatites and grenstone xenoliths in the southern part of the Barberton Mountain Land, South Africa. Precambrian Research 11, 373–397.

Beakhouse, G.P., Lin, S., Kamo, S.L., 2011. Magmatic and tectonic emplacement of the Pukaskwa batholith, Superior Province, Ontario, Canada. Canadian Journal of Earth Sciences 48, 187–204.

Belcher, R.W., Kisters, A.F.M., 2006. Progressive adjustments of ascent and emplacement controls during the incremental construction of the 3.1 Ga Heerenveen batholith, South Africa. Journal of Structural Geology 28, 1406–1421.

Belcher, R.W., Kisters, A.F.M., Poujol, M., Stevens, G., 2005. Structural emplacement of the 3.2 ga Nelshoogte pluton: implications for the origin of dome-and-keel structures in the Barberton granite-greenstone terrain. Geocongress, Durban.

Clemens, J.D., Yearron, L.M., Stevens, G., 1996. Barberton (South Africa) TTG magams: geochemical and experimental constraints on source-rock petrology, pressure of formation and tectonic setting. Precambrian Research 151, 53–78.

Condie, K.C., 1981. Archaean Greenstone Belts. : Developments in Precambrian Geology, 3. Elsevier.

De Ronde, C.E.J., Kamo, S.L., 2000. An Archaean arc-arc collisional event: a short-lived (Ca 3 Myr) episode, Weltevredeb area, Barberton greenstone belt, South Africa. Journal of African Earth Sciences 30, 219–248.

Diener, J., Stevens, G., Kisters, A.F.M., Poujol, M., 2005. Metamorphism and exhumation of the basal parts of the Barberton greenstone belt, South Africa: constraining the rates of mid-Archaean tectonism. Precambrian Research 143, 87–112.

Dziggel, A., Armstrong, R.A., Stevens, G., Nasdala, L., 2005. Growth of zircon and titanite during metamorphism in the granitoid-gneiss terrane south of the Barberton greenstone belt, South Africa. Mineralogical Magazine 69, 1019–1036.

Dziggel, A., Stevens, G., Poujol, M., Anheusser, C.R., Armstrong, R.A., 2002. Metamorphism of the granite-greenstone terrane south of the Barberton greenstone belt, South Africa: an insight into the tectono-thermal evolution of the “lower” portions of the Onverwacht Group. Precambrian Research 114, 221–247.

Ernst, W.G., Liu, J., 1998. Experimental phase-equilibrium study of Al- and Ti-contents of calcic amphibole in MORB — a semi-quantitative thermobarometer. American Mineralogist 83, 952–969.

Foley, S., Tiepolo, M., Vannucci, R., 2002. Growth of early continental crust controlled by melting of amphibolite in subduction zones. Nature 417, 837–840.

García-Casco, A., Lázaro, C., Rojas-Agramonte, Y., Kröner, A., Torres-Roldán, R.L., Núñez, K., Neubauer, F., Millán, G., Blaznco-Quintero, I., 2008. Partial melting and counterclock-wise P–T path of subducted oceanic crust (Sierra des Convento mélange, Cuba). Journal of Petrology 49, 129–161.

Graham, C.M., Powell, R., 1984. A garnet-hornblende geothermometer — calibration, testing and application to the Pelona schist, southern California. Journal of Metamorphic Geology 2, 13–31.

Grapes, R.H., Hoskin, P.W.O., 2004. Epidote group minerals in low-medium pressure metamorphic terranes. Reviews in Mineralogy and Geochemistry 56, 301–345.

Hartel, T.H.D., Pattison, D.R.M., 1996. Genesis of the Kaspuskasing (Ontario) migmatitic mafic granulites by dehydration melting of amphibole: the importance of quartz to reaction progress. Journal of Metamorphic Geology 14, 591–611.

Hollister, L.S., 1966. Garnet zoning: an interpretation based on the Rayleigh fractionation model. Science 154, 1647–1651.

Jahn, B.M., Glikson, A.Y., Peucat, J.J., Hickman, A.H., 1981. REE geochemistry and isotopic data of Archaean silicic volcanics and granitoids from teh Pilbara Block, Western Autstralia: implications for the early crustal evolution. Geochimica et Cosmochimica Acta 45, 1633–1652.

Johannes, W., 1983. On the origin of layered migmatites. In: Atherton, M.P., Gribble, C.D. (Eds.), Migmatites, melting and metamorphism. Shiva, Nantwich, pp. 142–162.

Kamo, S.L., Davis, D.W., 1994. Reassessment of Archaean crustal development in the Barberton Mountain Land, South Africa, bases on U-Pb dating. Tectonics 13, 167–192.

Kisters, A.F.M., Belcher, R.W., Poujol, M., Dziggel, A., 2010. Continental growth and convergence related arc plutonism in the Mesoarchaean: evidence from the Barberton granitoid greenstone terrain, South Africa. Precambrian Research 178, 15–26.

Kisters, A.F.M., Stevens, G., Dziggel, A., Armstrong, R.A., 2003. Extensional detachment faulting and core-complex formation in the southern Barberton granite-greenstone terrain, South Africa: evidence for a 3.2 Ga orogenic collapse. Precambrian Research 127, 355–378.

Le Bayon, B., Pitra, P., Ballèvre, M., Bohn, M., 2006. Reconstructing P–T paths during continental collision using multi-stage garnet (Gran Paradiso nappe, Western Alps). Journal of Metamorphic Geology 24, 477–496.

Lowe, D.R., 1994. Accretionary history of the Archean Barberton Greenstone Belt (3.55–3.22 Ga), southern Africa. Geology 22, 1099–1102.

Lowe, D.R., Byerly, G.R., Heubeck, C., 1999. Structural Divisions and Development of the West-central Part of the Barberton Greenstone Belt: Geol.Soc.Am.Spec.Pap., 329, pp. 37–82.

Martin, H., 1987. Petrogenesis of Archaean trondhjemites, tonalites and granodiorites from eastern Finland — major and trace element geochemistry. Journal of Petrology 28, 921–953.

Mehnert, K.R., 1968. Migmatites and the origin of granitic rocks. Elsevier, 393pp.

Moyen, J.F., 2011. The composite Archaean grey gneisses: petrological significance and evidence for a non-unique tectonic setting for Archaean crustal growth. Lithos 123, 21–36.

Moyen, J.F., Stevens, G., 2006. Experimental constraints on TTG petrogenesis: implications for Archean geodynamics. In: Benn, K., Mareschal, J.C., Condie, K.C. (Eds.), Archean geodynamics and environments: AGU Geophysical Monograph, 164, pp. 149–175.

Moyen, J.F., Stevens, G., Kisters, A., 2006. Record of mid-Archaean subduction from metamorphism in the Barberton terrain, South Africa. Nature 442, 559–562.

Namur, O., Charlier, B., Toplis, M.J., Higgins, M.D., Liégeois, J.P., Vander Auwera, J., 2010. Crystallisation sequence and magma chamber processes in the ferrobasaltic Sept Iles layered intrusion, Canada. Journal of Petrology 51, 1203–1236.

Petrelli, M., Poli, G., Perugini, D., Peccerillo, A., 2005. Petrograph: a new software to visualize, model and presenr geochemical data in igneous petrology. Geochmistry, Geophysics, Geosystems 6, Q07011, http://dx.doi.org/10.1029/2005GC000932.

Pitra, P., Kouamelan, A.N., Ballèvre, M., Peucat, J.J., 2010. Palaeoproterozoic high-pressure granulite overprint of the Archean continental crust: evidence for homogeneous crustal thickening (Man Rise, Ivory Coast). Journal of Metamorphic Geology 28, 41–58.

Prouteau, G., Scaillet, B., 2003. Experimental constraints on the origin of the 1991 Pinatubo dacite. Journal of Petrology 44, 2203–2241.

Proyer, A., 2003. The preservation of high-pressure rocks during exhumation : metagranites and metapelites. Lithos 70, 183–194.

Rapp, R.P., Watson, E.B., 1995. Dehydration melting of metabasalt at 8–32 kbar: implications for continental growth and crust-mantle recycling. Journal of Petrology 36, 891–931.

Robb, L.J., Barton Jr., J.M., Kable, E.J.D., Wallace, R.C., 1986. Geology, geochemistry and isotopic characteristics of the Archaean Kaap Valley pluton, Barberton mountain land, South Africa. Precambrian Research 31, 1–36.

Schmidt, M.W., 1992. Amphibole composition in tonalite as a function of pressure — an experimental calibration of the Al-in-hornblende barometer. Contributions to Mineralogy and Petrology 110, 304–310.

Schmidt, M.W., Thompson, A.B., 1996. Epidote in calcalkaline magmas; an experimental study of stability, phase relationships, and the role of epidote in magmatic evolution. American Mineralogist 81, 462–474.

Stevens, G., Moyen, J.-F., 2007. Metamorphism in the Barberton Granite Greenstone Terrain: a record of Paleoarchean accretion. In: Van Kranendonk, M.J., Smithies, R.H., Bennett, V. (Eds.), Earth's Oldest rocks. Elsevier, pp. 669–698.

Stormer, J.C., Nicholls, J., 1978. XLFRAC: a program for the interactive testing of magmatic differentiation models. Computers and Geoscience 4, 143–159.

Taylor, J., Stevens, G., 2010. Selective entrainment of peritectic garnet into S-type granitic magmas: evidence from Archaean mid-crustal anatectites. Lithos 120, 277–292.

Vielzeuf, D., Schmidt, M.W., 2001. Melting reactions in hydrous systems revisited: application to metapelites, metagreywackes and metabasalts. Contributions to Mineralogy and Petrology 141, 251–267.

Williams, M.L., Hanmer, S., Kopf, C., Darrach, M., 1995. Syntectonic generation and segregation of tonalitic melts from amphibolite dikes in the lower crust, Striding–Athabasca mylonite zone, northern Saskatchewan. Journal of Geophysical Research 100, 15717–15734.

Wolf, M.B., Wyllie, P.J., 1993. Garnet growth during amphibolite anatexis: implications of a garnetiferous restite. Journal of Geology 101, 357–373.

Wolf, M.B., Wyllie, P.J., 1995. Liquid segregation parameters from amphibolite dehydration melting experiments. Journal of Geophysical Research 100, 15611–15621.

Xiong, X.L., Adam, J., Green, T.H., 2005. Rutile stability and rutile/melt HFSE partitioning during partial melting of hydrous basalt: implications for TTG genesis. Chemical Geology 218, 339–359.